

ISOPHOT - PHOTOMETRIC CALIBRATION OF POINT SOURCES

B. Schulz¹, S. Huth^{1,2}, U. Kinkel^{1,2*}, D. Lemke²,
J. Acosta^{1,2,3}, M. Braun^{1,2,6}, H. Castañeda^{1,2,3}, L. Cornwall^{1,4}, C. Gabriel¹,
I. Heinrichsen^{1,5,7}, U. Herbstmeier², U. Klaas^{1,2}, R. Laureijs¹, T. Müller^{1,2}

¹ ISO Data Centre, ESA Astrophysics Division, Villafranca del Castillo, Spain

² Max-Planck-Institut für Astronomie, Heidelberg, Germany

³ Instituto de Astrofisica de Canarias, Tenerife, Spain

⁴ Rutherford Appleton Laboratory, Chilton, UK

⁵ Max-Planck-Institut für Kernphysik, Heidelberg, Germany

⁶ Astrophysikalisches Institut Potsdam, Germany

⁷ Infrared Processing and Analysis Center, JPL, Pasadena, USA

ABSTRACT

We discuss the photometric calibration of ISOPHOT for point sources in the wavelength range from 3.2 to 240 μm for the aperture photometer and the FIR camera section. To correct for temporal drifts of the detector responsivities, all observations included reference measurements of stable internal sources. These have been absolutely calibrated in-orbit against well known celestial standards comprising of stars, asteroids and planets. Corrections were derived for other non-ideal effects like nonlinearities, signal-transients, time-variable dark-current or misalignments. We use the overall consistency of the calibration tables with the measured data and the accuracy of the celestial standards to derive typical accuracies that can be achieved for staring- or raster-observations in standard configurations. With point-source observations and the use of standard apertures for the aperture photometer a baseline is defined, which will serve as a reference for the calibration of further instrument modes like chopped, multi-aperture or extended source measurements.

Key words: ISO; infrared astronomy; calibration; data-reduction; ISOPHOT.

1. INTRODUCTION

The imaging spectro photopolarimeter ISOPHOT (Lemke et al. 1996) onboard ESA's Infrared Space Observatory ISO (Kessler et al. 1996) features extrinsic photoconductors as infrared detectors, made from doped Silicon and Germanium. Since the detectors exhibit a varying response to IR-radiation, mostly due to cosmic particle hits, an internal fine calibration source (FCS) is used as stable reference. Electrical heating of the FCS with powers of 0.001

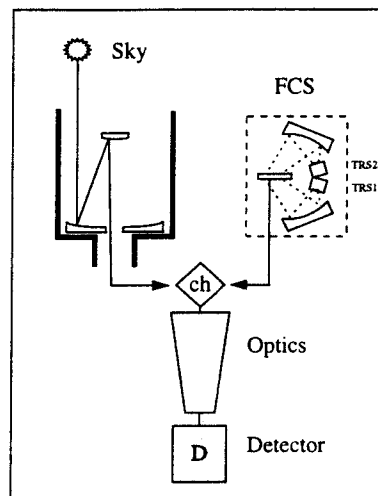


Figure 1. Schematic instrument setup from the calibration point of view. The detector receives IR-light from the sky and from the internal calibration source (FCS), switching beams with the chopper-mirror. Stability of the detector is only required for the time interval of both measurements.

to 50 mW, generates a range of highly reproducible fluxes over more than 5 orders of magnitude.

2. CALIBRATION SCHEME

By observing known celestial sources together with subsequent measurements of the FCS, set up to emit similar fluxes, we calibrated the FCS absolutely over the full accessible flux-range of the 25 filter bands as outlined in Figure 1. In turn the routine astronomical observing sequences were calibrated by attaching

*deceased 1997

at least one FCS-measurement to each sequence, that allowed to reestablish the detector responsivity $R = I_{phot}/P_{src}$ for the time of the observation, i.e. the ratio between measured photocurrent and corresponding infrared inband-power on the detector. We calculate the inband-power for standard point-sources as $P_{src} = A_{tel} f_{PSF_{f,a}} T_{refl} \int [T_f(\lambda) R_p(\lambda) F(\lambda)] d\lambda$, where A_{tel} is the area of the telescope primary, $f_{PSF_{f,a}}$ the fraction of the light of a point-source falling into the detector-aperture a for the selected filter f , T_{refl} the reflection losses of all mirrors in the optical path, $T_f(\lambda)$ the spectral transmittance of the filters and field-lenses, $R_p(\lambda)$ the relative spectral response function of the detector-pixel p , normalised to the peak-response, and $F(\lambda)$ the spectral energy distribution of the point-source. Note that including $R_p(\lambda)$ makes the detector responsivity R filter-independent for the same detector pixel. We ignore the small systematic error arising from the simplified colour independent PSF correction-factor.

To convert inband-powers to flux-densities F_ν , for the normal case of objects with initially unknown SED, the relation $P_{src} k_f = F_\nu C1_f f_{PSF_{f,a}}$ is used, where the conversion factors $C1$ are calculated for an assumed reference spectrum of $\nu F_\nu = const$. The result on the left still needs to be divided by the factor k_f to correct to the actual colour of the object once this is known.

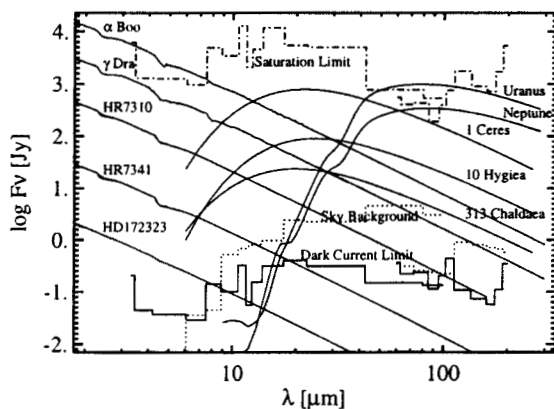


Figure 2. The coverage of the flux-domain accessible to ISOPHOT by celestial standards. Examples of each of the three source-types are plotted as solid lines (c.f. Tables 1 and 2 for relative brightnesses). Dashed lines mark the upper flux-limits and the typical limits due to IR-background and dark-current.

3. CELESTIAL STANDARDS

The photometric calibration of ISOPHOT is based entirely on point-sources, which constitute the best known infrared fluxes in the sky. The sources are observed either with PHT-P in a standard aperture that is defined per filter (23 arcsec for 3.3-7.7 μ m, 52 arcsec for 10-16 μ m, 79 arcsec for 20-25 μ m and 180 arcsec for 60-100 μ m), or with PHT-C in each pixel of the array detectors. As the detailed radiation spectrum

Table 1. The list of stars used for ISOPHOT calibration. The brightnesses are given in the P_{11.5} and C₆₀ filters, depending on the usage in the range 3-30 μ m or 45-240 μ m respectively. The magnitudes were calculated with respect to the photometric system defined by the ISOPHOT filters with the Kurucz model of Vega as zero-point.

Name	2nd name	type	mag (P _{11.5})	mag. (C ₆₀)
HD172323	-	F9V	6.55	
HD184400	-	F5	7.53	
HR337	β And	M0IIIv	-2.05	-2.17
HR617	α Ari	K2III	-0.76n	-0.83
HR1457	α Tau	K5III		-3.12
HR1654	ϵ Lep	K5IIIv		-0.43
HR3748	α Hya	K3II-III	-1.31	-1.39
HR5340	α Boo	K1III	-3.15	-3.22
HR5886	-	A2IV	5.09	
HR5986	-	F8IV-V	2.71	
HR6514	-	A4V	6.14	
HR6688	-	K2III		0.92
HR6705	γ Dra	K5III	-1.46	-1.56
HR6847	-	G2V	4.76	
HR7001	α Lyr	A0V	0.00	
HR7310	-	G9III	0.67	0.67
HR7341	-	K1III	3.64	
HR7451	-	F7V	4.51	
HR7469	-	F4V	3.51	
HR7633	-	K5II-III	1.14	1.11
HR7742	-	K5III	2.18	
HR7980	ω Cap	M0III		-0.08
HR8684	-	G8III	1.27	
HR8775	β Peg	M2.5II-I	-2.44	-2.54

of the FCS was unknown and linearity of the detectors could not a priori be postulated, the empirical FCS-calibration required the availability of calibration standards covering the full observable flux-range between 3 and 240 μ m. The upper flux-limit is determined by the cold readout electronics (CRE) and the detector responsivity. The lowest signals are determined by the celestial background (Zodiacal Light, Galactic Cirrus) and at short wavelengths by the dark-current. Figure 2 shows these limits projected into the flux-domain. The flux/wavelength-range between is well covered by stars, planets and asteroids.

Important aspects of the selection of standard stars were non-variability, no stellar companion, no infrared-excess, low background and good visibility to ISO over the mission. The ISO Ground Based Preparatory Program (GBPP) (Jourdain de Muizon & Habing 1992, Van der Blik et al. 1992, Hammersley et al. 1998) provided spectra up to wavelengths of 50 μ m, calculating Kurucz stellar model atmosphere grids from J, H, K and L narrow-band photometry in combination with either the Infrared Flux Method (Blackwell et al. 1991) or the V-K versus T_e relation (Di Benedetto 1993, Di Benedetto 1995) and the surface gravities and metallicities of Cayrel De Strobel et al. (1992). FIR extrapolations were provided too. In the range between 2 and 160 μ m the SEDs have attributed uncertainties between 3 to 5 per cent. Above 160 μ m all quoted errors are 5 per cent. Another calibration programme by Cohen et al. (1995) provided SEDs in the range of 1.2 to 35 μ m by splicing together measured spectral frag-

Table 2. The list of planets and asteroids used for the calibration in the 45-240 μm range. We give the range of magnitudes occurring during visibility intervals of the given object over the ISO-mission.

Solar System Standards		
#	source name	mag (C.60)
	Uranus	-7.21...-7.28
	Neptune	-6.01...-6.07
1	Ceres	-5.85...-6.46
2	Pallas	-4.23...-5.67
3	Juno	-3.81...-4.36
4	Vesta	-5.34...-6.03
10	Hygiea	-3.52...-3.97
54	Alexandra	-3.13...-3.42
65	Cybele	-2.69...-3.24
106	Dione	-1.32...-1.35
313	Chaldea	-2.10...-2.15
532	Herculina	-2.91...-3.99

ments of cool K and M-stars. The fragments were absolutely calibrated against black-bodies. The measured composite-SEDs are used to derive so-called template-SEDs for fainter stars (Cohen et al. 1996), assuming that the spectral shape depends only on the spectral type and the luminosity class. The absolute flux level is set by NIR-photometry. To extrapolate to 240 μm , Engelke functions together with effective temperatures from Blackwell et al. (1991) were used. The typical absolute accuracy of the templates is about 3 per cent, while the FIR-extensions longward of 25 μm are assigned 6 per cent. Both programs used Kurucz model-atmospheres of Sirius and Vega as common zeropoint for their broadband photometry. Table 1 lists the stars that were actually used for ISOPHOT calibration.

Uranus and Neptune are commonly used as sub-millimeter and FIR standards (e.g. Griffin & Orton 1993). They provided the highest calibrated flux-levels between 45 and 200 μm . Mars, Jupiter and Saturn were already too bright for ISOPHOT. Model-SEDs of both planets were kindly provided for all dates of ISOPHOT observations by Abbas et al. (1997). The models take into account temperature profiles, CH_4 -mixing ratios and absorption by H_2 and He. These were obtained directly from Voyager IRIS and RSS instrument data, supplemented by model profiles from Abbas et al. (1997) or taken from Lindal (1992) for Neptune. Comparison with other models for Uranus (Griffin & Orton 1993) and for Neptune (Lellouch 1997), showed consistency within 10-20 per cent between 240 and 30 μm . Larger discrepancies appear below 30 μm in a regime, where H_2 and He-absorption becomes a major factor.

The brighter Asteroids are well enough understood by thermophysical modelling, to be able to predict an SED with an accuracy of ± 10 per cent. Therefore they can fill the gap at intermediate flux-levels, that appears at wavelengths between 45 and 200 μm between Planets and Stars (see fig 2). Some specific complications arise, since they are moving objects w.r.t. the sky-background and show periodic variations of their intensity due to rotation and varying distance to the Earth and Sun. For the actual photometric calibration the Thermophysical Model (TPM) (Müller & Lagerros 1998) is used. The TPM assumes

a rotating ellipsoid, thus accounting for lightcurve variations, and parametrises heat conduction, surface roughness and scattering in the regolith. A database of asteroid fluxes was collected not only from literature and ground-based observations, but also from ISOPHOT-cross-calibrations with stars. The calibration of the ground based observations applied the same stellar SEDs as ISOPHOT. The JCMT calibration used planet models. The fundamental parameters like radius, albedo, spin-vectors etc. were determined either from literature or from fits of the TPM to the asteroid fluxes. The final accuracy of the standards is ± 10 per cent in the wavelength range from 24 to 500 μm , except for 106 Dione and 65 Cybele, where discrepancies between model and observations of 20-30 per cent were found. Table 2 lists the solar-system objects, that were actually used for ISOPHOT calibration.

4. DATA REDUCTION

Each calibration observation consisted of 4 different measurement types: on-source, off-source, heated FCS and cold FCS. The data was reduced automatically by a dedicated software package as described in Huth & Schulz (1998), using PIA as a basis (Gabriel et al. 1997). Reducing the measured integration ramps homogeneously to signals in units of V/s, i.e. S_{src} , S_{bck} , S_{fcs} , S_{str} respectively, it applies the standard corrections for ramp-nonlinearities, signal dependence on readout-timing and glitches. Moreover it includes an automatic transient correction algorithm and a quality flag system. For each FCS-measurement the inband-power corresponding to the FCS-heating-power h is calculated according to $P_{fcs}(h) = \frac{(S_{fcs}(h) - S_{str}) P_{src}}{S_{src} - S_{bck}}$. This assumes linearity of the detector over the flux-range spanned by the measurements of celestial standard and FCS. The results form the basis for the derivation of several calibration tables and further investigation of calibration issues.

5. PHOTOMETRIC CALIBRATION

The fundamental calibration tables are called FCS-power-curves and contain the relation between FCS heating-power h and FCS-inband-power P_{fcs} . They are determined directly from the data by polynomial fits for each of the 25 filter bands. For the aperture photometer the table $P_{fcs}(h)$ is expressed in units of $[\text{W}/\text{mm}^2]$ since the FCS appears as an extended source. The values are multiplied by the area A of the field-aperture, to derive the FCS-inband-power on the detector. This works yet strictly only for the standard apertures, since the illumination of the apertures is not perfectly homogeneous. Systematic deviations appear for different apertures, therefore the results presented here do only apply for the standard apertures. For the array detectors the FCS-power-curves are already in units of $[\text{W}]$, however since they too are illuminated inhomogeneously by the FCS, the average power-curve needs to be corrected for each individual pixel by the illumination-matrix $\Gamma_{p,f}$. This matrix depends also on filter. The

responsivity R as defined above is independent of filter. Systematic differences found between different filters of the same detector-pixel, independent of the celestial standard, are corrected by the filter-to-filter correction table $\chi_{p,f}$. These corrections are different for different pixels of the same array-detector, which is likely due to spatial inhomogeneities across the broadband filters.

Using the derived tables of calibration parameters, an ISOPHOT observation of a point-source is calibrated as follows. First, the responsivity of each detector pixel is determined from the FCS-measurement. For P-detectors according to:

$$R_p = \frac{(S_{fcs,p,f} - S_{str,p,f}) C_{int}}{P_{FCS,f}(h) A \chi_{p,f}} \quad (1)$$

and for C-detectors according to:

$$R_p = \frac{(S_{fcs,p,f} - S_{str,p,f}) C_{int}}{P_{FCS,f}(h) \Gamma_{p,f} \chi_{p,f}} \quad (2)$$

We use 90 fFarad for the value of the integration capacity of the CRE C_{int} , except for C200, where it is 140 fFarad. The FCS-straylight signal $S_{str,p,f}$ was always measured in the calibration observing sequences, but was not measured in every astronomical observing sequence. In general it is close to the dark-current signal and can be replaced by it. Only C200 shows some correlation of the straylight-signal with the background signal.

Next the sky-signals $S_{p,f}$ are converted into an inband-power by

$$P_f = \frac{S_{p,f} C_{int}}{R_p \chi_{p,f}} \quad (3)$$

Note that the source-measurement does not need to be in the same filter band as the FCS-measurement, however, if so, $\chi_{p,f}$ cancels out and the systematic uncertainty associated with this table is removed from the error budget. The conversion to flux density is performed as explained above.

6. UNCERTAINTIES

We assess the overall consistency of the FCS-calibration by comparing the FCS-power-curves and the datapoints they were derived from. Since the calibration observations passed the same reduction steps as every science observation, the scatter is representative for the photometric uncertainty of staring- or raster-observations. Uncertainties of the celestial calibration standards (section 3) increase the scatter. Only a photometric bias among the standards would not be seen. Table 3 shows the scatter that was calculated as the standard deviation of all values $P_{Cal-G}(h)/P_{meas}(h) - 1$ of one filter, where P_{Cal-G} is the inband-power from the FCS-power-curve and P_{meas} is the corresponding measured one. For the array detectors C100 and C200 the scatter calculation included all pixels. The flux range of each detector was divided into an upper and a lower part to account for the gradual increase of the scatter towards smaller fluxes, which is mainly due to larger

Table 3. Comparison of derived FCS-power-curves with measured calibration data. n is the number of measurements used, max is the maximum deviation found in per cent, σ_{lo} and σ_{hi} are the standard deviations in per cent for the low- and high-part of the fluxes.

detector	n	max per cent	σ_{lo} per cent	σ_{hi} per cent
P1	148	47	14	10
P2	54	72	16	5
P3	93	77	26	21
C100	1788	146	18	14
C200	878	54	14	8

noise and increasing contribution by the background uncertainty. For multi-filter measurements the uncertainty of the filter-to-filter calibration matrices χ of 2 to 9 per cent has to be included into the overall error budget.

ACKNOWLEDGMENTS

We like to thank M. Abbas, M. Cohen, P. Hammersley, D. Osip and C. Telesco for their support, in particular the many SEDs of calibration standards. Furtheron we thank all our colleagues at VILSPA and MPIA for their efforts to make ISO a success.

REFERENCES

- Abbas, M., Osip, D., Romani, P. 1997, priv. comm.
- Di Benedetto, G. P. 1993, A&A, 270, 315
- Di Benedetto, G. P. 1995, ApJ, 452, 195
- Blackwell, D. E., Lynas-Gray, A. E., & Petford, A. D. 1991, A&A, 245, 567
- Van Der Blik, N.S., et al. 1992, ISO., Messenger, 70, 28
- Cayrel De Strobel, G., et al. 1992, A&AS., 95, 273
- Cohen, M., et al. 1995, AJ, 110, 275
- Cohen, M., Witteborn, F.C., et al. 1996, AJ, 112, 2274
- Gabriel, C., et al. 1997, Proc. of the ADASS VI conference, eds. Hunt, G. & Payne, H.E., p. 108
- Griffin, M. J. & Orton, G. S. 1993, Icarus, 105, 537
- Hammersley, P. L., et al. 1998, A&AS, 128, 207
- Huth, S. & Schulz, B., 1998, ASP Conf. Ser. 145: Astronomical Data Analysis Software and Systems VII, 7, 212
- Kessler, M.F., Steinz, J.A., Anderegg, M.E., et al. 1996, A&A, 315, L27
- Lellouch, E., 1997, priv. comm.
- Lemke, D., Klaas, U., et al. 1996, A&A, 315, L64
- Lindal, G. 1992, AJ, 103, 967
- Müller, T. & Lagerros, J. 1998, A&A, 338, 340-352
- Jourdain de Muizon, M. J.-D., Habing, H. 1992, Les Houches Series: Infrared Astronomy with ISO, Th. Encrenaz, M.F. Kessler eds., pp 129-138